Intermetallics 121 (2020) 106770

Contents lists available at ScienceDirect

Intermetallics

journal homepage: http://www.elsevier.com/locate/intermet

Fatigue crack threshold analysis of TiAl SENT and CC specimens – Influence of starter notch and precracking

S. Eck [a,*], J. Maierhofer [a], C. Tritremmel [a], H.-P. Gaenser [a], S. Marsoner [a], N. Martin [b], R. Pippan [c]

[a] Materials Center Leoben Forschung GmbH, Roseggerstraße 12, 8700, Leoben, Austria
[b] Rolls-Royce Plc, Derby, DE24 8BJ, UK
[c] Erich Schmid Institute of Materials Science, Austrian Academy of Sciences, 8700, Leoben, Austria

ARTICLE INFO

Keywords:
TiAl
Cyclic fatigue testing
Crack propagation
Elevated temperature

ABSTRACT

Due to their low density, excellent high temperature strength and good oxidation resistance, TiAl alloys are being used for components in commercial aero-engines. Fatigue crack threshold analysis is a safety critical input to the component design. Fatigue properties of a TiAl alloy with a near fully lamellar microstructure were investigated in detail by means of fatigue crack growth testing. Two different types of standard fatigue specimens (SENT – single edge notch tension and CC – corner crack) were machined and subjected to cyclic loading at temperatures between room temperature and 700 °C with a stress ratio R = 0.1. The present work examines the influences of sample geometry, starter notch width, starter notch radius and the effect of compression precracking on the measured threshold stress intensity factor range ΔK_{th}. The results show to which extent the different specimen geometries and starter notch preparations yield the same fatigue crack growth (FCG) threshold results and which setup yields in the most conservative results, i.e. lowest crack growth thresholds for the same material and load condition.

1. Introduction

In a recent article, Rugg et al. outlined the material life cycle opportunities and threats for high temperature application of titanium alloys in gas turbines [12]. New concepts of aero-engines such as the Rolls-Royce UltraFan target towards significant reduction of Specific Fuel Consumptions (SFC) via radically new engine designs. Rugg et al. describe the challenges of the corresponding material development for safety critical engine parts.

Measurements of the fatigue crack growth (FCG) threshold stress intensity factor range ΔK_{th} performed at the loads and temperatures that are expected in the corresponding engine part are an important input to the design process of the parts. In this work, we focus on the ΔK_{th} assessment for TiAl components that typically endure high cyclic loading at high temperatures.

Within the defined ISO standard for fatigue testing [3] there are a several methods for measuring the ΔK_{th} of a specific material. One of the differences in these methods is the choice of the specimen geometry for the FCG tests.

Yang et al. investigated the microstructure and tensile properties of hot isostatic pressed (HIP) Ti4522XD powders in 2012 [16]. In 2014, the same research group published fatigue crack growth fracture surfaces of corner crack (CC) FCG specimen of the same material tested at 650 °C [17].

Pippan et al. Schloffer et al. and Leitner et al. investigated fatigue crack growth in TiAl alloys of different compositions using singe edge notch tension (SENT) specimens [4,8,13]. Mine et al. also used this specimen geometry to investigate the effect of the lamellar spacing on fatigue crack growth behavior of a TiAl-alloy [6]. Similar experiments have also been performed and reported in Refs. [1,2,14].

When comparing the starter notch preparation it is apparent that all authors who used SENT specimens for FCG analyses applied a fatigue precracking procedure as recommended by the ISO standard, whereas those authors who used corner-crack specimen geometries did not apply a pre-crack procedure.

Compression precracking of SENT specimens is described in Ref. [7a, 7b], whereby at small load amplitudes the crack growth rate decreases with increasing crack length until the crack arrests. By step wise increasing the load amplitude, the R-curve for the threshold and the standard da/dN vs. ΔK curve can be determined.

In corner crack specimens the notch depth is usually small, hence the necessary stress to generate a precrack becomes high, with the risk of

* Corresponding author.
E-mail address: sven.eck@mcl.at (S. Eck).

https://doi.org/10.1016/j.intermet.2020.106770
Received 26 August 2019; Received in revised form 9 March 2020; Accepted 9 March 2020
Available online 8 April 2020

plastic buckling during the precracking. Therefore, other techniques are usually applied. For the material used in the present work, a ΔK of 26 MPa $m^{-1/2}$ was necessary to initiate a pre-crack in the SENT-specimen geometry (for the dimensions see the section below). To obtain the same ΔK for the CC-specimen geometry one would have to apply compressive forces up to 20 kN; that implies that for a cross section of 25 mm^2 compressive stresses of 800 MPa would occur.

Some authors prepare the starter notch via electro discharge machining, whereas others apply mechanical machining (diamond saw, razor blade, …). To clarify the influence of starter notch geometry and precracking on the resulting fatigue crack thresholds, SENT and CC specimens of the same TiAl alloy, 4522XD, were prepared with different starter notches and subsequently tested at room temperature and at elevated temperatures up to 700 °C in ambient air in the same testing device.

2. Experimental setup

2.1. Material

Ti4522XD casting stock was centrifugally cast into molds that were subsequently subjected to a HIP and heat treatment cycle. Microstructure investigations on both SENT and CC specimens (exemplary image given in Fig. 1) showed the same microstructure as published by Yang et al., in 2013, i.e. a microstructure "composed of fine lamellar colonies with an average lamellar colony size of about 100 μm and a maximum grain size of 240 μm" [17].

2.2. Specimen geometries, starter notch preparations and precracking

For the present work, SENT specimens and CC specimens with different starter notch geometries were used. The variations resulted in 5 different specimen types, i.e. standard corner crack specimens ("CC"), compression precracked SENT specimens ("SENT CP"), SENT specimens with starter notches via electro discharge machining with small notch ("SENT EDs") and wide notch ("SENT EDw") and SENT with a razor blade polished notch ("SENT RB"). The corresponding SENT and CC specimen dimensions are summarized in Table 1.

2.2.1. Notch preparation and precracking for SENT-CP specimens

For "SENT CP" specimens, the standard procedure for notch preparation has been taken from Ref. [4,8]: A starter notch was prepared via electro discharge machining (EDM) with a 250 μm wire and refined via razor blade polishing. As illustrated in Fig. 2a and b, the resulting EDM cut was 4 mm deep and 350 μm wide, the razor blade polishing resulted in a 70 μm deep and 25 μm wide notch. Subsequently, the SENT specimens were subjected to a compression pre cracking resulting in a typically 100 μm long pre-crack, as shown in Fig. 2c. The precracking was performed at a load ratio R = 20 and a corresponding ΔK which was chosen as small as possible to initiate a fatigue pre-crack. Pre-tests showed that at least 26 MPa $m^{1/2}$ was necessary to initiate a pre-crack in Ti4522XD SENT specimen. The length of the produced pre-crack fulfills the geometrical requirements of the standard. The used notch root radii and the notch opening angle are very small, hence the requirement that an imaginary notch with an opening angle of 30° located at the crack tip of the pre-crack should never touch the real notch was always fulfilled, for details see the ISO standard [3] as well as the ASTM standard E561.

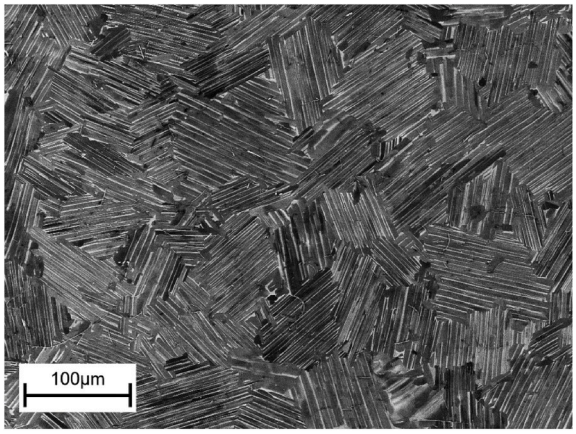

Fig. 1. SEM micrograph of the investigated Ti4522XD.

Table 1
Dimensions of the different specimens and starter notches used in the present work.

	"SENT CP" (standard SENT)	"SENT EDs"	"CC"
Specimen length	80 mm	80 mm	65 mm
Specimen thickness B	6 mm	6 mm	
Specimen width W	20 mm	20 mm	
Gauge length cross section			5 mm × 5 mm
Notch depth	4 ± 0.1 mm	4 ± 0.1 mm	0.5 ± 0.1 mm
notch width	20–30 μm	40–50 μm	40–50 μm
Pre-crack length	100–150 μm	none	none

2.2.2. Notch preparation for CC specimens

For CC specimens, the standard procedure for notch preparation has been taken from Ref. [16,17]. A starter notch was prepared on the corner of the CC specimens using a fine EDM cut, i.e. an EDM cut with a 30 μm wire. Images of a typical resulting notch are shown in Fig. 2d–f.

In [17] Yang et al. stated "*Many fine cracks were generated during the re-cast process of EDM at the notch surface and they can be 10 μm in depth. The fine cracks form an almost continuous network. During testing those with the favorable orientations will propagate under certain stress conditions.*" The image shown in Fig. 2f confirms this statement, with the exception that the network of cracks is not continuous. Furthermore, it shows that the EDM re-solidified zone in the TiAl specimen was approx. 10–15 μm wide and that many cracks penetrated right through that re-solidified zone. As in the paper by Yang et al. [17], no compression precracking procedure was applied to the corner crack specimen.

2.2.3. EDM notched SENT specimens

For a better estimation of the influence of the starter notch preparation with and without precracking procedure starter notches were prepared in SENT specimens with the fine 30 μm EDM wire ("SENT EDs") and the coarse 250 μm EDM wire ("SENT EDw") and the specimens were subsequently tested without the precracking procedure.

Fig. 2g shows the starter notch geometry for "SENT EDs". Cutting a 4000 μm long notch in a 6 mm wide specimen with a 30 μm EDM wire was technically challenging and a considerably low cutting speed had to be used. As a result, the EDM notch in this specimen was considerably wider than the one in the corner crack specimens, i.e. the resulting notch width was ~100 μm (Fig. 2h). The SEM backscatter detector (BSD) images in Fig. 2f and i show that the EDM machining resulted an approx. 15 μm wide rough surface corresponding to the re-solidified zone and that various cracks can be detected in the re-solidified zone.

2.3. Fatigue crack growth in notches prepared via EDM

To investigate the fatigue crack initiation in notches prepared via EDM, a "SENT EDs" specimen was investigated in a scanning electron microscope (SEM) with the same settings before and after the FCG testing. The resulting SEM images are displayed in Fig. 3.

The SEM images in Fig. 3 clearly indicate the presence of microcracks in the remelt-zone of the EDM. In this specimen the fatigue

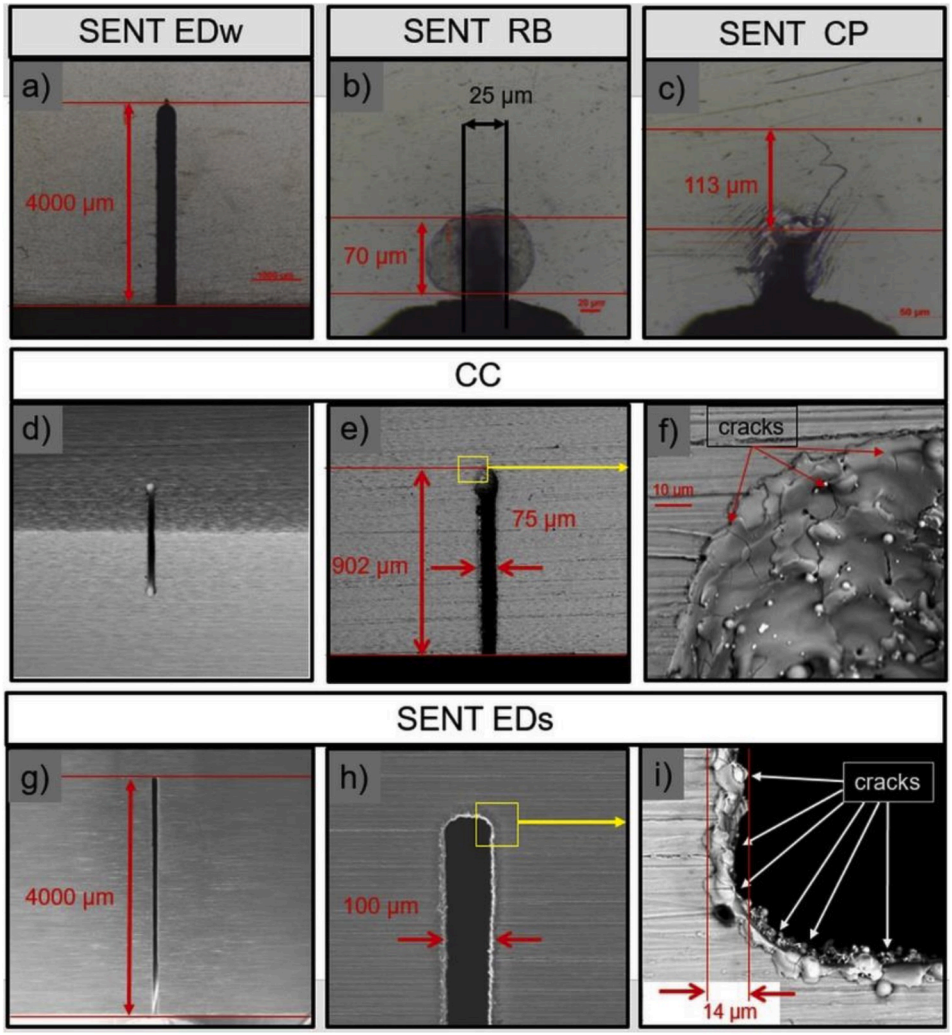

Fig. 2. SEM images of the various starter notches prepared in TiAl specimens.
"standard SENT" (a–c): a) "SENT EDw": 4 mm deep and 350 µm wide EDM cut, b) "SENT RB": 70 µm deep and 25 µm wide razor blade polished cut, c) SENT CP: 113 µm long pre-crack after the compression precracking;
"standard CC" (d–j) d) CC EDM notch at the corner, e) CC EDM notch on one side 800 µm long and 75 µm wide, f) SEM-BSD image of the notch root showing micro-cracks in the re-solidified zone of the EDM cut in the CC specimen;
"SENT EDs" (g–h): g) 4 mm long EDM cut prepared with a 30 µm wire, h) resulting notch width of 100 µm, i) SEM-BSD image of the notch root showing micro-cracks in the 14 µm wide re-solidified zone of the EDM cut.

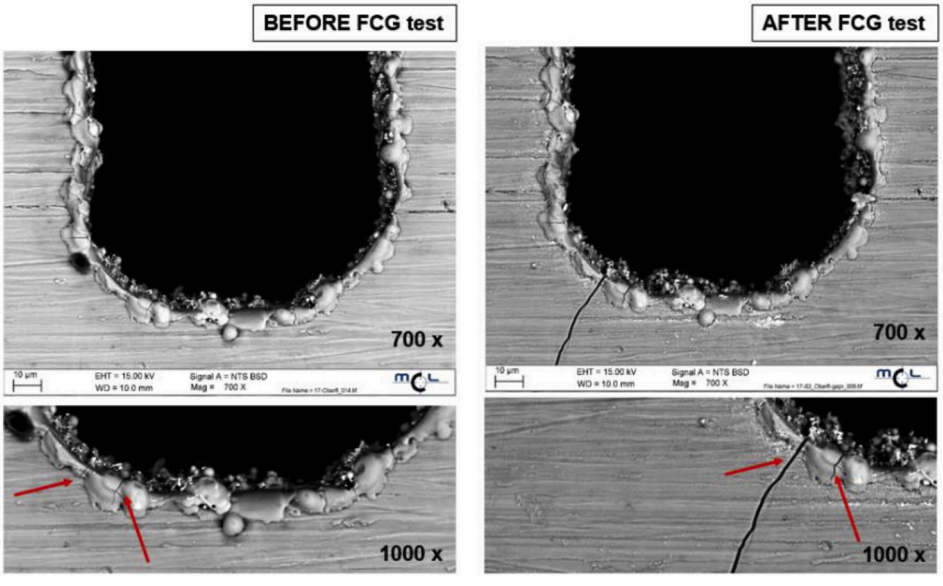

Fig. 3. SEM images of a "SENT EDs" specimen before (left) and after (right) the FCG testing.

crack grew from one of these micro-cracks, i.e. the one, where the combination of local load, crack driving force and local microstructure (orientation of the lamellar microstructure, see Ref. [17]) yielded the lowest crack resistance.

2.4. Testing equipment and temperature control

The fatigue crack growth experiments were performed in ambient air using a resonant testing machine equipped with a high temperature furnace. The temperature control via the two-stage oven was calibrated for each testing temperature between 25 °C (RT) and 800 °C with a specimen equipped with spot welded thermocouples as shown in Fig. 4. This setup resulted in a temperature accuracy better than ±1 °C in the specimen gauge length section for the whole temperature range.

The resonant testing machine was operated with a testing frequency of approximately 85 Hz in load-controlled mode. The crack growth was monitored using the direct current potential drop (DCPD) technique using a direct current of 2 A. Any temperature influence on the measured electric potential drop due to the Seebeck effect at bimaterial junctions was excluded by periodic switching of the direction of the electric current and subsequent averaging. Crack arrest was defined as the (averaged) crack growth rate falling below a value of at most 6×10^{-8} mm/cycle (see next section).

2.5. Testing procedure and evaluation of the crack growth threshold ΔK_{th}

The experiments were conducted under step-wise increasing constant loads as proposed by Tabernig [15] and following the guideline for experimental determination of a cyclic R-curve published in more detail in Ref. [5]. For load amplitudes which correspond to ΔK values smaller than the effective threshold $\Delta K_{\text{eff th}}$ no crack propagation is observed. For load amplitudes which correspond to ΔK values larger than $\Delta K_{\text{eff th}}$, the crack starts to propagate. The crack grows initially, but after a certain crack extension a crack arrest occurs due to the build-up of crack tip shielding mechanisms (crack deflection, crack bridging and crack closure) [11]. Subsequently, the load is increased so that the crack can grow further. As soon as the crack starts to grow through, one gets the crack growth curve. At that crack extension, crack tip shielding mechanisms have already built up completely.

Fig. 5 shows a plot of the applied force amplitude and the corresponding potential drop measured during subsequent load cycles with R = 0.1 on a 4522XD CC specimen at 400 °C.

The DCPD potential value was recorded every 5 s; for the given testing frequency of 85 Hz, each data point hence corresponds to 425 load cycles. The statistical scatter/measurement accuracy of the potential measurement was in the order of ±0.5 μV corresponding to a crack length change of ± 5 μm.

At the lower force amplitude, the constant potential value indicates that no crack growth occurs for >75,000 cycles. For this specific specimen, increasing the force amplitude from 1550 N to 1750 N led to a significant increase in the measured potential indicating crack growth. This load step corresponded to 25 MPa for this specimen geometry and this specific specimen fractured after 1192 data points, i.e. 506600 load

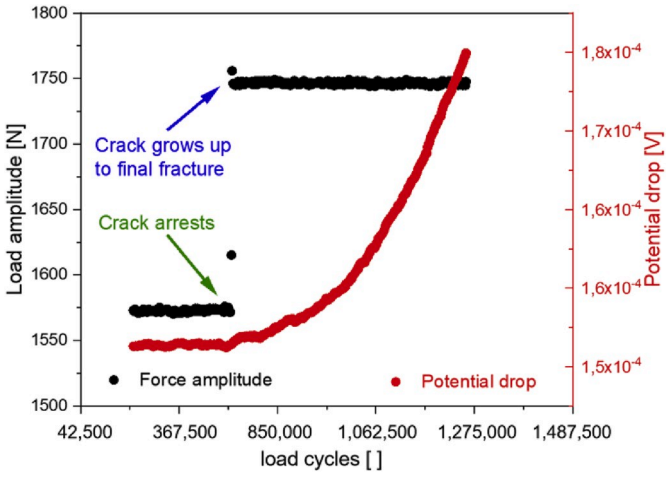

Fig. 5. Illustration of the last load step where the crack arrest takes place during a step-wise load increasing testing procedure. Left scale, black dots: plot of the force amplitude vs. load cycles, right scale, red dots: plot of the corresponding potential measured with the DCPD technique.

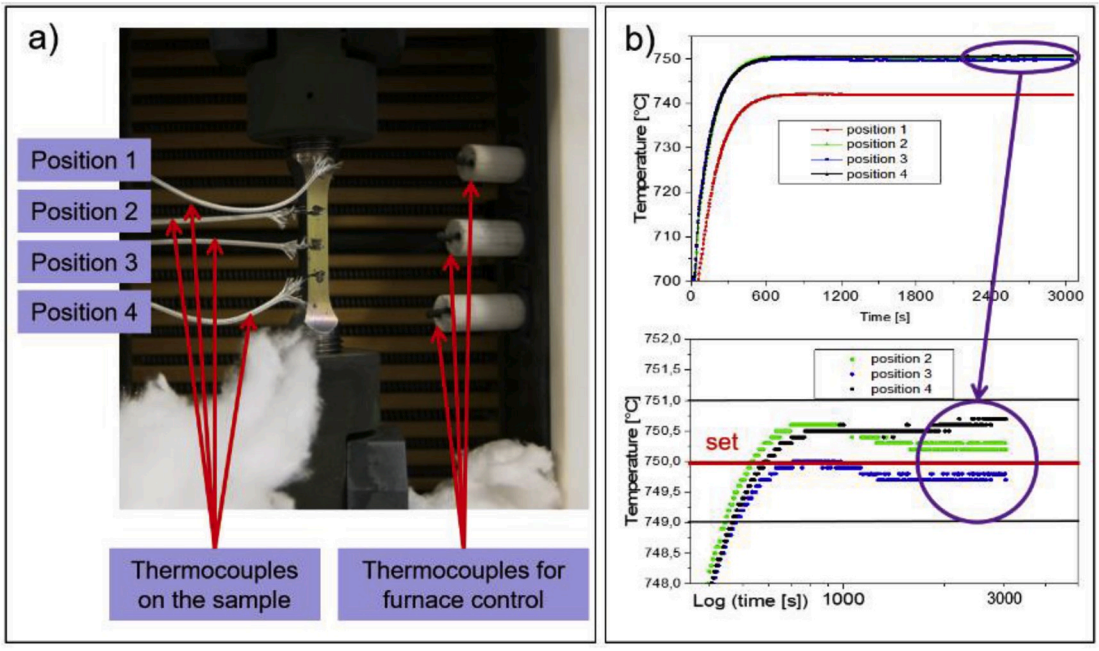

Fig. 4. Illustration of the temperature calibration and control via thermocouples a) Image of the thermocouples spot-welded to a CC specimen for calibration and the thermocouples in the furnace used for the temperature control; b) Temperature-time plots of the corresponding setup for 750 °C set temperature.

cycles at 1750 N force amplitude.

Fig. 6 shows the data given in Fig. 5 after calculating the stress intensity factor ΔK (based on the compliance function given in Ref. [3]) as a plot of the crack growth per load cycle da/dN versus the stress intensity factor ΔK. For details on the test procedure see Ref. [8]. Tabernig et al. [15] correlate the short crack growth measurements and the crack growth threshold evaluation with the long crack growth measurements, i.e. da/dN vs. ΔK, as shown in Ref. [16,17].

The plot illustrates that the crack growth threshold value ΔK_{th} for this specific specimen, testing temperature and load case was somewhere between 4.7 MPa $m^{-1/2}$, i.e. the load step where the last crack arrest takes place and 5.3 MPa $m^{-1/2}$, i.e. the load step where the crack grew until final fracture. Note that these values are given as the lower and upper bound of the crack growth threshold values ΔK_{th} in the following tables for each tested specimen. Additionally, we performed a standard fatigue crack growth experiment applying the load shedding technique. This load shedding experiment delivered a ΔK_{th} of 5.34 MPa $m^{-1/2}$, which is in an exceptionally good agreement with the upper limit obtained in the step wise load increasing experiments. This indicates that in the stepwise load increasing test in the last load step the crack tip shielding mechanisms are nearly fully developed.

3. Results and discussion

3.1. The influence of the notch geometry

To analyze the influence of the starter notch geometry, fatigue crack growth tests were performed at room temperature at a stress ratio R = 0.1 with SENT CP (compression precracked), SENT EDs (EDM notch with small notch width), SENT EDw (EDM notch with a wide notch width), SENT RB (EDM notch with sharp razor blade polished notch) and CC samples (with a small EDM notch). The results of the da/dN vs. ΔK curves obtained in a stepwise increasing load amplitude test are shown in Fig. 7.

For the calculation of ΔK the details of the notch geometry have not been taken into account. The crack length in all cases assumed as $a = D + l$, where D is the depth of the notch and l is the real physical crack length, as illustrated in a sketch in Fig. 8a.

3.1.1. "SENT EDw" and "SENT RB"

The highest ΔK_{th} has been obtained in the "SENT RB" and "SENT EDw" samples despite the large difference in the SENT EDw root radius compared to the micro crack free sharp razor blade polished notch in SENT RB. In the razor blade polished notch a crack has to be generated, whereas in the EDM notch the growth conditions for the microcrack in the notch stress field has to be fulfilled.

Only for physical crack lengths l larger than $\rho/2$, where ρ is the notch root radius, the standard geometry parameters for the K calculation are a really good approximation. For smaller l the standard equations, taking not into account the notch geometry, overestimate ΔK [7a,7b], as illustrated in Fig. 8b. This overestimation is more pronounced in the specimen with the 350 μm notch root radius (SENT EDw).

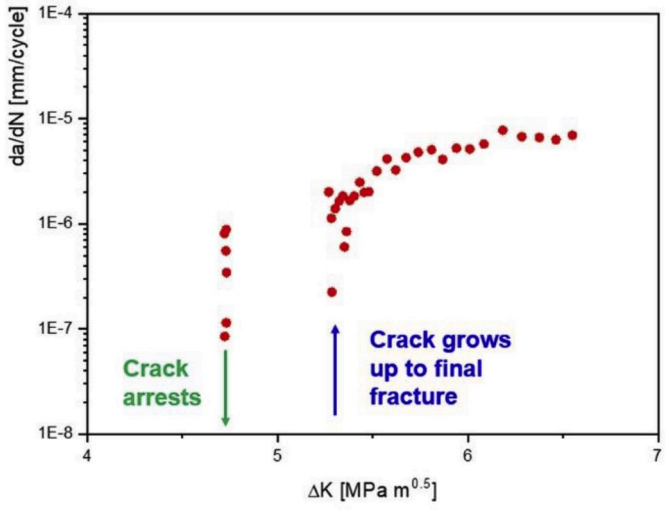

Fig. 6. Plot of da/dN vs. stress intensity factor derived from the potential measurements shown in Fig. 5, for details on the test procedure see Ref. [8].

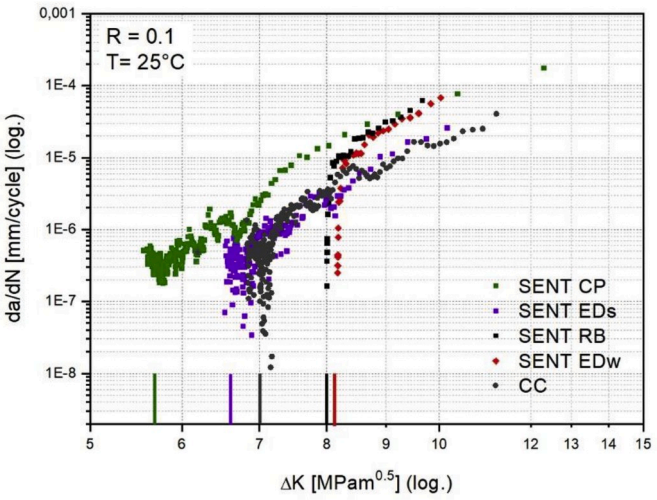

Fig. 7. Plots of da/dN vs. stress intensity factor measured at room temperature and R = 0.1: Results of 4 SENT specimens with different starter notch geometries and a standard CC specimen are displayed with different colors.

3.1.2. "SENT EDs" and "CC"

In the samples with the small EDM notch, ("SENT EDs" and "CC") this overestimation is relatively small. The somewhat larger apparent ΔK_{th} in the CC and SENT EDs specimen are mainly caused by the reason that the microcracks at the EDM notch root do not form a through thickness crack. This is evident if one compares the R curves for ΔK_{th} in Fig. 7. Furthermore, one has to take into account the difference in the stress intensity factor range (more accurately in the geometry parameter) for a through-thickness crack and a micro-crack of the same depth on the notch root as schematically shown in Fig. 8c. The geometry parameter of a through thickness crack is approx. 1.5 times larger than the geometry parameter of a semicircular crack of the same depth. This should also contribute to a somewhat larger ΔK_{th} in CC specimens. The effect is not as pronounced as one would expect from the simple notch crack shape analyses due to the short crack effect on the R-curve.

3.1.3. "SENT EDs" and "SENT CP"

The R curve of ΔK_{th} of "SENT EDs" is significantly steeper than the one of "SENT CP". One reason might be that a tensile residual stress field induced by the compression precracking (despite the very small load amplitude) induces a shift of the R curve to larger crack extensions [15]. However, the main reason is the difference in the pre-crack geometry. The pre-crack generated by cyclic compression is a real through thickness crack, whereas at the root of the EDM notch a large number of non-connected microcracks are present at the start of the fatigue crack growth experiment. The first observed crack extension in the EDM notched sample is observed at significant larger ΔK and the extension before crack arrest is quite small. Even at the ΔK value where the last arrest of the crack is observed, the extension is only about 20 μm, which is smaller than the colony size. Hence, even at this load amplitude no through thickness crack had been generated. In the next load amplitude step where ΔK is larger than the long crack threshold a through thickness crack is formed and no further stopping of the crack propagation

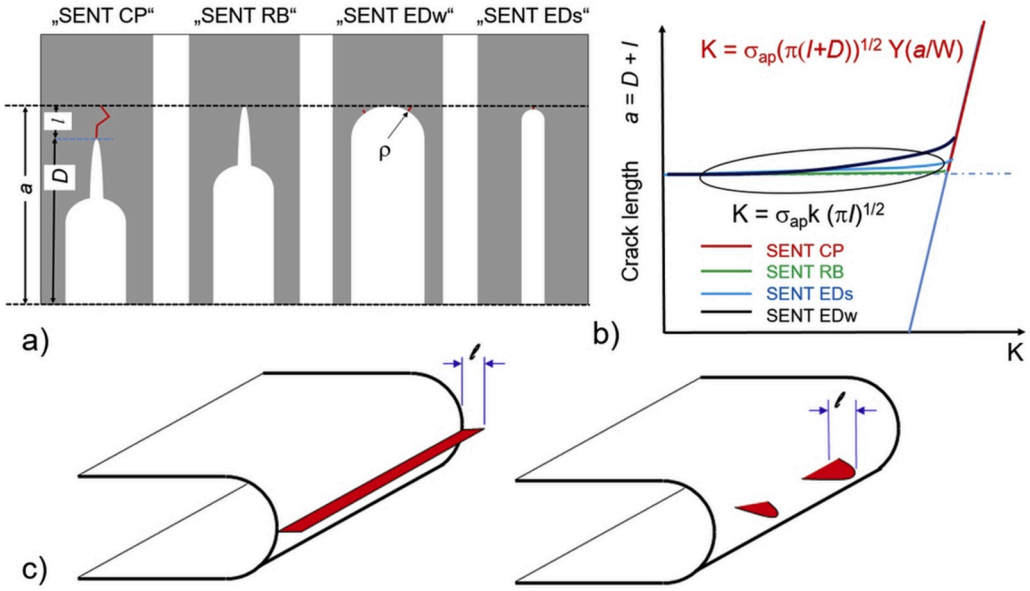

Fig. 8. a) Sketch illustrating the variations in the notch and the resulting crack lengths a for the SENT specimens, b) sketch illustrating the correlation between the dimensions a, D, l and the resulting stress intensity factor K, c) illustration of the difference of a through-thickness crack and a micro-crack at the notch root.

takes place.

To sum up, the threshold and the R-curve of the threshold determined on compression pre-cracked samples results in the most conservative values for ΔK_{th}. The EDM generated test samples without precrack can overestimate the cyclic load bearing capacity of TiAl components containing cracks.

3.2. Temperature dependence of ΔK_{th} in SENT and CC specimens

Stepwise increasing load amplitude tests have been performed on CC and compression precracked SENT specimens (SENT CP) in order to determine the ΔK_{th} variation as a function of temperature at R = 0.1. In Fig. 9 the ΔK values were plotted as a function of test temperature for both specimen types. Dots correspond to the maximum non-propagating and minimum propagating stress intensity range for 2 specimens per temperature and specimen geometry, dashed lines indicate the corresponding mean values.

The temperature behavior of ΔK_{th} of the SENT samples exhibits the typical behavior of this type of TiAl alloys [13] with a minimum of ΔK_{th} at about 400 °C. The reason for this behavior seems to be that the different contributions to the threshold of stress intensity range have a different temperature dependence.

The separation of the intrinsic and extrinsic mechanisms [11] and the separation of the different extrinsic mechanism are not as well defined as in ductile materials [9,10]. In order to obtain a guide for the eye, a schematic picture of the contributions to ΔK_{th} is given in Fig. 10.

With increasing temperature, the contribution of crack bridging decreases. The authors assume that at low temperature the bridges deform predominately elastically, whereas at higher temperatures the increase of cyclic plastic deformation of the bridges results in a fatigue failure of the bridges. Consequently, the contribution of bridge shielding deceases. The difference in ΔK_{th} of the CC and SENT samples supports this assumption regarding the decrease of crack bridging contribution with increasing temperature. In the CC specimens, ΔK_{th} is controlled by the coalescence of the microcracks at the EDM notch root. If the fatigue of the bridges between the microcracks is easier at higher temperature, the ΔK_{th} values of the CC and SENT specimens should become smaller, as it is observed in this study. The increase of ΔK_{th} at higher temperatures is to the author's opinion caused by an increase of oxide induced crack closure. This is supported by a clearly visible development of the oxide layer in the high temperature experiments and fits very well to the results and explanations given by M. Schloffer in his PhD thesis [13].

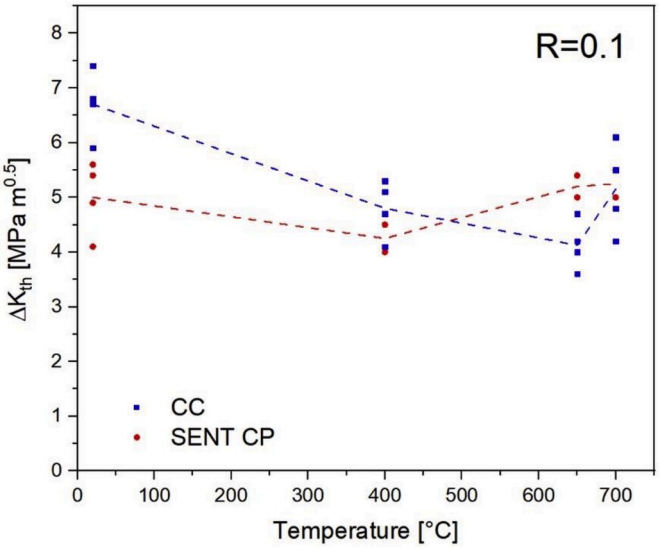

Fig. 9. Plots of maximum non-propagating and minimum propagating stress intensity range for 2 specimens per temperature and specimen geometry. Dashed lines indicate the corresponding mean values for "SENT CP" and "CC" specimens.

4. Summary

Ti4522XD, a TiAl alloy with a near fully lamellar microstructure was investigated by means of fatigue crack growth tests.

To analyze the influence of the starter notch geometry, fatigue crack growth tests were performed at room temperature at a stress ratio R = 0.1 on 5 different specimen types, i.e. standard compression precracked SENT specimens, standard corner crack specimens (without compression precrack) and SENT specimens without compression precrack but varying EDM starter notch geometries. The results showed that the compression precracked SENT delivers the smallest ΔK_{th}, i.e. the most conservative values. Threshold values determined on EDM notches in CC

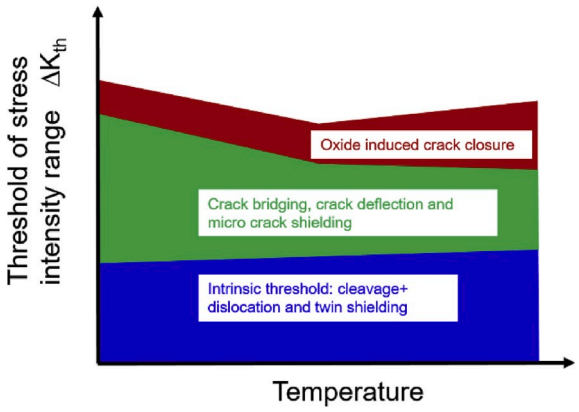

Fig. 10. Schematic picture of the contributions to ΔK_{th}.

and SENT specimens are somewhat larger.

To investigate the influence of the specimen geometry on the obtained ΔK_{th} in the typical temperature range of aero engine turbine parts, FCG tests were performed at temperatures between room temperature and 700 °C with a stress ratio R = 0.1.

The difference in the ΔK_{th} determined in compression precracked SENT specimens and CC specimens is larger at room temperature and becomes relatively small at temperatures larger than 400 °C. The threshold of stress intensity factor range has a minimum in the medium temperature range of ~400 °C. The first decrease of ΔK_{th} is most probably induced by a decrease of crack tip shielding due to crack bridging and at the higher temperature, the increase of ΔK_{th} is caused by increase of oxide induced crack closure.

CRediT authorship contribution statement

S. Eck: Project administration, Writing - original draft, Writing - review & editing. **J. Maierhofer:** Data curation, Formal analysis. **C. Tritremmel:** Investigation, Methodology, Visualization. **H.-P. Gaenser:** Conceptualization, Software. **S. Marsoner:** Methodology, Validation. **N. Martin:** Conceptualization, Resources. **R. Pippan:** Writing - review & editing, Supervision.

Acknowledgement

The authors gratefully acknowledge the financial support by the EU Horizon 2020 program within the Joint undertaking CleanSky2 project "TiAlCracks" (Project No 686711) and by the COMET program within the K2 Center "Integrated Computational Material, Process and Product Engineering (IC-MPPE)" (Project No 859480). This program is supported by the Austrian Federal Ministries for Transport, Innovation and Technology (BMVIT) and for Digital and Economic Affairs (BMDW), represented by the Austrian research funding association (FFG), and the federal states of Styria, Upper Austria and Tyrol.

Appendix A. Supplementary data

Supplementary data to this article can be found online at https://doi.org/10.1016/j.intermet.2020.106770.

References

[1] S. Beretta, et al., Analysis of fatigue damage accumulation in TiAl intermetallics, Key Eng. Mater. 592–593 (2013) 30–35. https://doi.org/10.4028/www.scientific.net/kem.592-593.30. Trans Tech Publications, Ltd., Nov.
[2] M. Filippini, S. Beretta, L. Patriarca, G. Pasquero, S. Sabbadini, Defect tolerance of a gamma titanium aluminide alloy, Procedia. Eng. 10 (2011) 3677–3682, https://doi.org/10.1016/j.proeng.2011.04.605.
[3] International Standard ISO 12108:2018(E), Metallic materials — fatigue testing —fatigue crack growth method. https://www.iso.org/standard/42815.html.
[4] T. Leitner, M. Schloffer, S. Mayer, J. Eßlinger, H. Clemens, R. Pippan, Fracture and R-curve behavior of an intermetallic β-stabilized TiAl alloy with different nearly lamellar microstructures, Intermetallics 53 (2014) 1–9, https://doi.org/10.1016/j.intermet.2014.04.005.
[5] J. Maierhofer, S. Kolitsch, R. Pippan, H.P. Gänser, M. Madia, U. Zerbst, The cyclic R-curve – determination, problems, limitations and application, Eng. Fract. Mech. 198 (2018) 45–64, https://doi.org/10.1016/j.engfracmech.2017.09.032.
[6] Y. Mine, K. Takashima, P. Bowen, Effect of lamellar spacing on fatigue crack growth behaviour of a TiAl-based aluminide with lamellar microstructure, Mater. Sci. Eng. 532 (2012) 13–20, https://doi.org/10.1016/j.msea.2011.10.055.
[7] (a) R. Pippan, The growth of short cracks under cyclic compression, Fatig. Fract. Eng. Mater. Struct. 9 (5) (1987) 319–328, https://doi.org/10.1111/j.1460-2695.1987.tb00459.x;
(b) R. Pippan, M. Berger, H.P. Stüwe, Influence of crack length on fatigue crack growth in deep sharp notches, Metall. Trans. 18A (1987) 429–435, https://doi.org/10.1007/BF02648804.
[8] R. Pippan, P. Hageneder, W. Knabl, H. Clemens, T. Hebesberger, B. Tabernig, Fatigue threshold and crack propagation in γ-TiAl sheets, Intermetallics 9 (2001) 89–96, https://doi.org/10.1016/S0966-9795(00)00111-4.
[9] R. Pippan, C. Zelger, E. Gach, C. Bichler, H. Weinhandl, On the mechanism of fatigue crack propagation in ductile metallic materials, Fatig. Fract. Eng. Mater. Struct. 34 (2011) 1–16, https://doi.org/10.1111/j.1460-2695.2010.01484.x.
[10] R. Pippan, S. Wurster, D. Kiener, Fracture mechanics of micro samples: fundamental considerations, Mater. Des. 159 (2018) 252–267, https://doi.org/10.1016/j.matdes.2018.09.004.
[11] R. Ritchie, Mechanisms of fatigue crack propagation in metals, ceramics and composites: role of crack tip shielding, Mater. Sci. Eng. 103 (1988) 15–28, https://doi.org/10.1016/0025-5416(88)90547-2.
[12] D. Rugg, M. Dixon, J. Burrows, High-temperature application of titanium alloys in gas turbines. Material life cycle opportunities and threats – an industrial perspective, Mater. A. T. High. Temp. 33 (4–5) (2016) 536–541, https://doi.org/10.1080/09603409.2016.1184423.
[13] M. Schloffer, Gefüge und Eigenschaften der intermetallischen TNM-Legierung/ Microstructure and properties of an intermetallic TNM-alloy, PhD thesis (German), Montanuniversität Leoben, 2013.
[14] Loris Jonathan Signori, Taiki Nakamura, Yotaro Okada, Ryosuke Yamagata, Hirotoyo Nakashima, Masao Takeyama, Fatigue crack growth behavior of wrought γ-based TiAl alloy containing β-phase, Intermetallics 100 (2018) 77–87, https://doi.org/10.1016/j.intermet.2018.04.024. ISSN 0966-9795.
[15] B. Tabernig, P. Powell, R. Pippan, Resistance curves for the threshold of fatigue crack propagation in particle reinforced aluminium alloys, in: J. Newman, R. Piascik (Eds.), Fatigue Crack Growth Thresholds, Endurance Limits, and Design, ASTM International), West Conshohocken, PA, 2000, pp. 96–108. https://www.astm.org/DIGITAL_LIBRARY/STP/PAGES/STP13428S.htm.
[16] C. Yang, D. Hu, X. Wu, A. Huang, M. Dixon, Microstructures and tensile properties of hot isostatic pressed Ti4522XD powders, Mater. Sci. Eng. 534 (2012) 268–276, https://doi.org/10.1016/j.msea.2011.11.068.
[17] J. Yang, H. Li, D. Hu, M. Dixon, Microstructural characterisation of fatigue crack growth fracture surfaces of lamellar Ti45Al2Mn2Nb1B, Intermetallics 45 (2014) 89–95, https://doi.org/10.1016/j.intermet.2013.10.011.